Observing Cross-Species Cross-Cancer Chemosensitivity Signatures with Dynamic-Contrast OCT

Dawith Lim^a, Zhen Hua^a, Zhe Li^a, Ali Ajrouch^b, Ahmad Karkash^b, Shadia Jalal^b, Michael Childress^c, John Turek^d, and David Nolte^a

^aDepartment of Physics and Astronomy, Purdue University, West Lafayette, Indiana 47907, USA

^bIndiana University School of Medicine, Department of Medicine, Indianapolis, Indiana, USA ^cDepartment of Veterinary Clinical Sciences, Purdue University, West Lafayette, Indiana 47907, USA

^dDepartment of Basic Medical Sciences, Purdue University, West Lafayette, Indiana 47907, USA

ABSTRACT

Despite improvements in the ability to treat cancer, first-line chemotherapy in standard-of-care treatments still fail to elicit a response from about half of cancer patients. This limitation signals a pressing need for practical methods to select personalized cancer therapies. Biodynamic imaging (BDI; a form of dynamic-contrast OCT with low-coherence digital holography) on living cancer biopsies from patients shows potential as a method to guide personalized selection of cancer therapy. However, building a library of signatures for different types of cancer has been a practical obstacle. Here, a comparative preclinical/clinical trial with two-species (human and canine) and two-cancers (esophageal carcinoma and B-cell lymphoma) demonstrates the general applicability of BDI as a method of chemoresistance prediction and as a viable tool for personalized medicine. This study identifies a set of drug response phenotypes that span species and cancer type, suggesting the existence of universal characteristics, which would reduce the burden of library construction needed for the method to be useful for doctors and their patients.

Keywords: OCT, Biodynamic imaging, holography, cancer

1. INTRODUCTION

Biodynamic imaging (BDI) is a full-frame, dynamic-contrast OCT (DC-OCT) method using off-axis digital holography in the far field.^{1–3} Light scattered from living samples yield highly dynamic speckle, which produce a wide Doppler frequency spread on monochromatic light caused by intracellular and cellular motion at broad scales⁴ ranging from slow, large scale membrane rearrangements and cell shape changes, moving at speeds of nanometers per second, up to fast organelle and vesicle transport at speeds of microns per second.

An important use case of BDI is in the prediction of a tumor's response to different chemotherapeutic drugs using biopsy samples taken from patients. This would enable doctors to identify a treatment regime tailored specifically for the patient, increasing the likelihood that the treatment will be effective. Both effective and ineffective treatment take a significant toll on the patient's health, and so it is important that the patient does not suffer unnecessarily by undergoing an ineffective treatment. Correlations between biodynamic signatures obtained using BDI to predict clinical outcomes have been observed independently in canine B-cell lymphoma,⁵ human epithelial ovarian cancer,⁶ and human bladder cancer,⁷ showing promise as a method for personalization of cancer treatment, but no comparative study had been done to explore the common spectral signatures across species and cancer types.

Further author information: (Send correspondence to David Nolte)

David Nolte: E-mail: nolte@purdue.edu

2. METHODS

2.1 Biopsy sample preparation

Pinch biopsies were collected from human and canine patients in pre-clinical and clinical trials, following protocols approved by Indiana University Medical school IRB and Purdue Animal Care and Use Committee, respectively. A portion of each biopsy was submitted for histopathologic confirmation of the disease, and the remainder of the biopsy was cut into smaller pieces (about 1mm³ in volume) and placed in 96-well plates for *ex-vivo* Biodynamic Imaging.

2.2 Dynamic-Contrast OCT

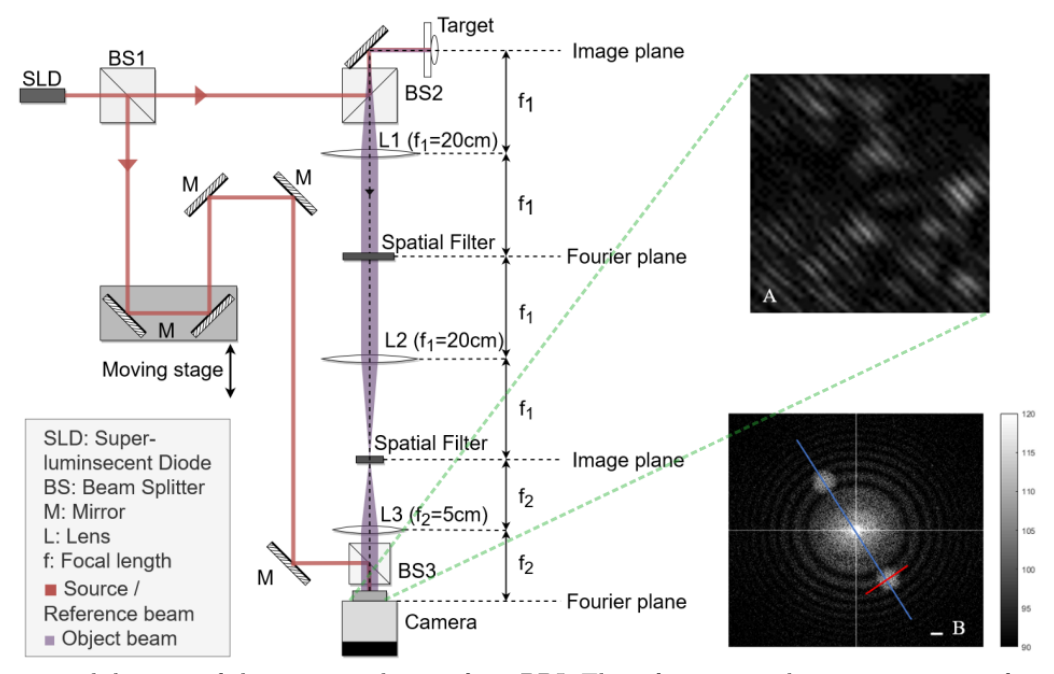


Figure 1. An optical diagram of the setup used to perform BDI. The reference arm has a moving stage for time-domain control the depth of sample section observed. The object arm has two spatial filters, one each in the image and the Fourier plane. Panel A: The raw hologram captured on the CMOS camera; Panel B: 2D FFT of the hologram showing the central 0th order peak and two side bands.

The samples were imaged using a Mach-Zehnder interferometer configured to perform Fourier domain off-axis digital holography (set up as shown in figure). Off-axis digital holography is a well established technique that allows a simultaneous recording of both intensity and phase information. The reference arm was fitted with mirrors on a moving stage to delay a short-coherence ($\sim 30~\mu m$) superluminescernt diode (SLD). This enables coherence gating, which is necessary to perform depth-resolved imaging through turbid media such as living tissue. The raw data acquired are 2D spatial transforms of the image.

To retrieve the object field, a 2D spatial Fast Fourier Transform (FFT) is performed on the intensity map of the interference pattern captured on the CMOS camera. Because the interference pattern is captured as intensity, the reconstructed image plane consists of two autocorrelation terms (one each for object beam and FFT of the reference beam) and two cross correlation terms (side bands) that are the image reconstruction. The reference beam is a monochromatic plane wave, so the reconstructed sidebands are the optical cross section of the target, offset from the center of the reconstruction due to the angle between the object and reference beams ($\sim 1^{\circ}$). The two side bands represent phase conjugate pairs, $O\delta$ and $O^*\delta$.

2.3 Post-Processing

From the reconstruction, we select one of the two side bands, and perform a time-domain FFT of the reconstruction over a stack of frames captured at 25fps. This gives the Doppler shift frequency spectrum of the sample, which manifest as intensity fluctuations of the reconstructed image. It does not matter which of the two side band is chosen, because the hologram captured on the CMOS is a real-valued intensity map, and so in performing the Fourier transform, Hermitian symmetry prevents us from identifying which of the two is the original and which is conjugated, unless additional information were supplied.

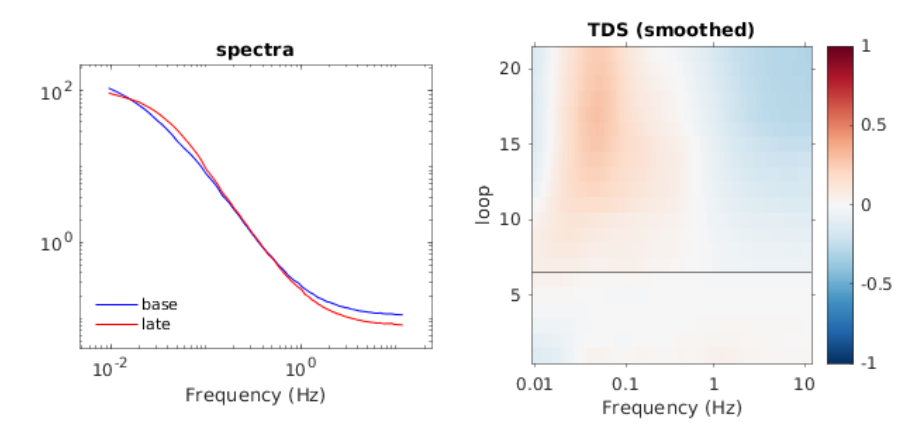


Figure 2. Left: Doppler shift frequency spectrum obtained from the reconstruction; Right: Spectrogram generated from the stack of spectra such as that shown in the left panel.

Finally, the Doppler shift frequency spectra are stacked over the course of an experiment at a 1 hour interval, subtracting the averaged baseline spectrum collected before treatment to construct a spectrogram. The spectrogram thus obtained provides a visual map of activity in the tissue that loosely correlates with the scale of dynamics involved, ranging from 0.01 Hz, which corresponds to movements on the order of the cell size, such as cell shape changes, large undulations in the membrane and cell death, up to 10Hz, which corresponds to the dynamics of small intracellular components such as vesicle transport. The mid-frequency range between 0.1Hz and 1Hz is associated with localized deformations of the cell membrane (e.g. endocytosis) and large-scale intracellular activities.

2.4 Analysis

To evaluate the predictive capability of the Doppler signatures for predicting patient response to therapy, a set of 40 features were derived from the data, as shown in figure 3. The set of 40 features encoding of the patterns constitute the feature vectors that were used as the input data for the machine learning inference.

To capture the relationship between these feature vectors and the patient's clinical outcome, a shallow feed-forward binary classifier with a single hidden layer consisting of 8 neurons was constructed. The model was then trained and validated against the clinical outcomes, following a 2-holdout cross-validation training routine, in which the neural net was trained on all but two randomly selected patients, and then validated on the two held out patients. This approach was taken because, by the nature of clinical trial, the sample size available was extremely limited. Because the spectrogram and its features are phenomenological and its mechanistic origins difficult to isolate, techniques such as machine learning that can identify complex, non-linear patterns that are not intuitively accessible were deemed ideal for the application. A shallow feed forward architecture was deployed because on one hand, it is small enough to avoid overfitting when training with such limited dataset, and on the other hand was just complex enough to be able to identify and parse the non-linear patterns present in our data.

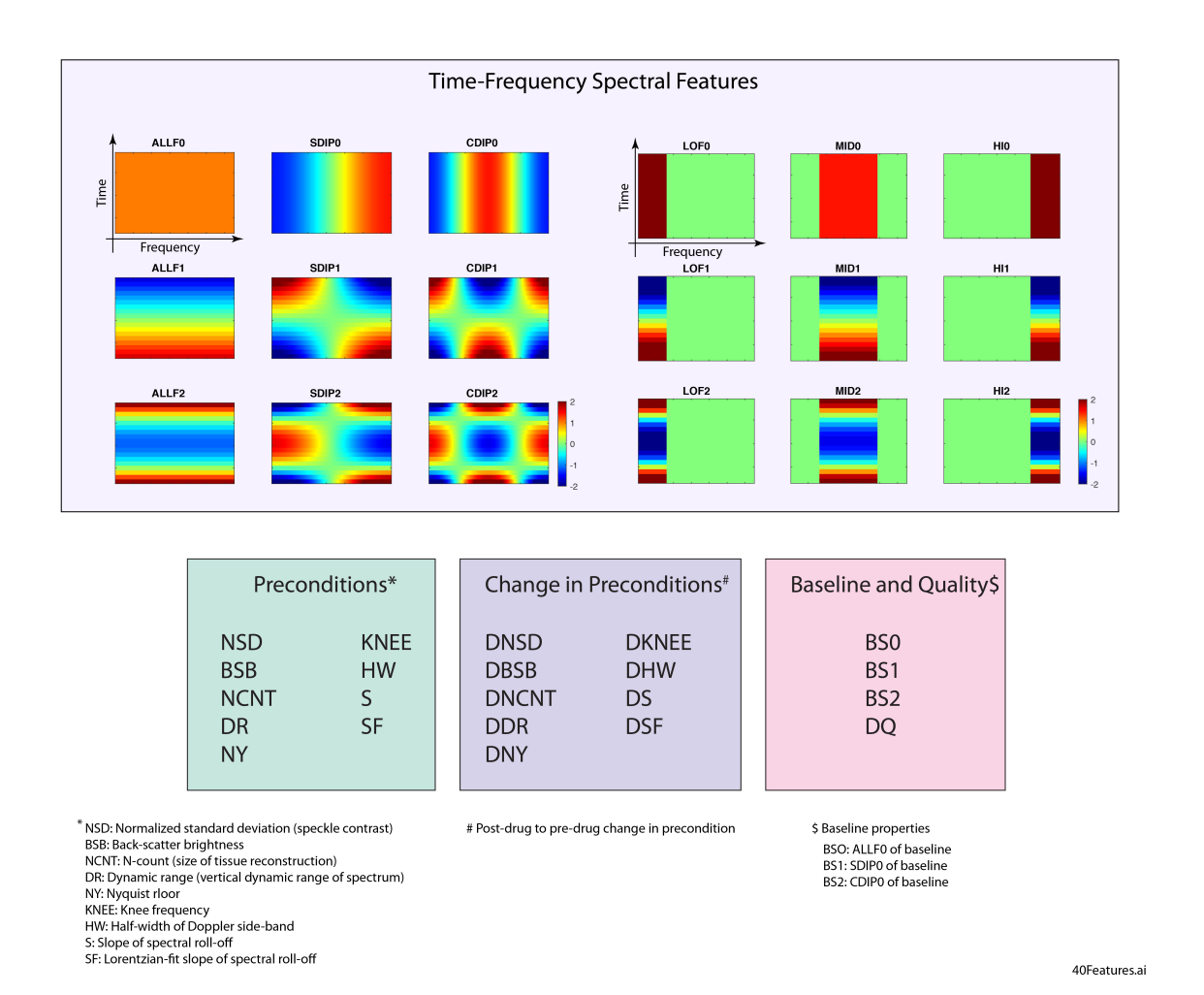


Figure 3. Categorization of the 40 biomarkers derived from the data. 18 encode graphical patterns that appear on the spectrogram, 18 encode characteristics of the reconstruction image, and the remaining four encode information about the quality of the data. Note that these biomarkers are not completely independent of each other.

3. RESULTS

We examined the cross-species, cross-disease phenotypic patterns in the data. Figure 4 highlights the similarity between the four phenotypes seen in human esophageal cancer and in canine B-cell lymphoma. Pheno 1 represents blue shifted wells (increased organelle activity), Pheno 2 represents red shifted (decreased metabolic activity), Pheno 3 represents mid-frequency enhanced (increased membrane activity) and Pheno 4 represents mid-frequency suppressed (often associated with apoptosis [25]). The fact that these four subgroups appear consistently across different patient cohort, host species and tumor type, suggests that these phenotypes are universal features rather than specific to particular sample type.

Next, we examined how much each phenotype affects the prediction performance, by selectively removing each phenotype from the data before going through the training and validation steps using the neural net. A notable result is showcased in ROCs shown in figure 5. Evidently, the elimination of phenotypes with low-frequency enhancements (red shifts) prior to the averaging led to a marked improvement in predictive performance of the biodynamic spectroscopy. Therefore, red-shifted wells should be excluded from analysis because they are not representative of the patient response to chemotherapy.

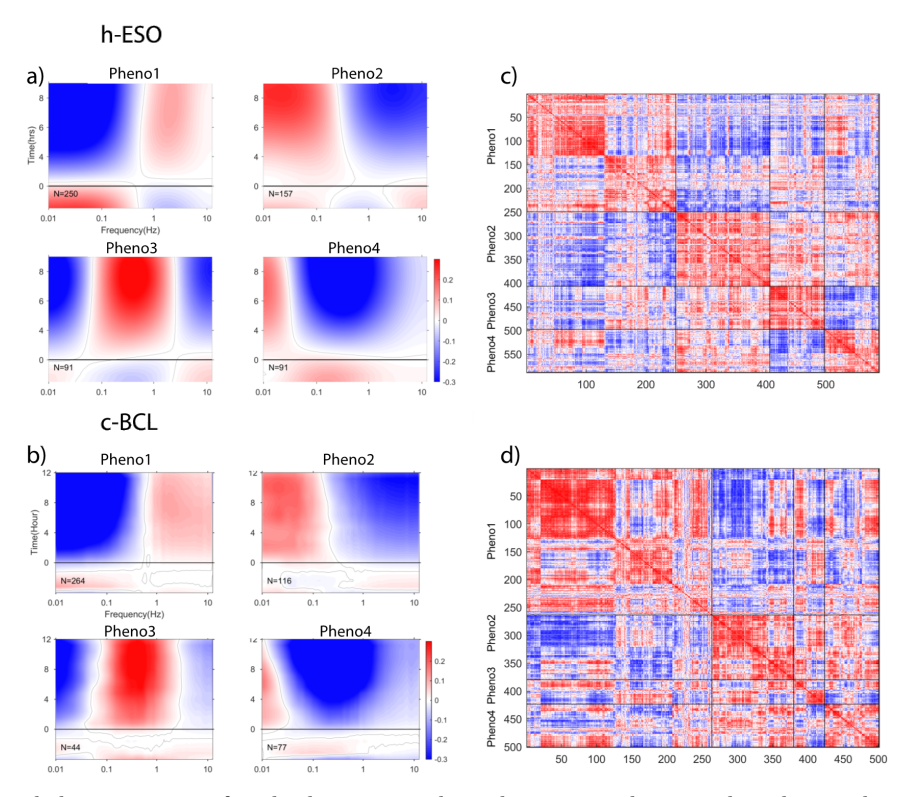


Figure 4. Well-based drug-responses for the human esophageal cancer and canine lymphoma clinical trial. Averaged spectrograms a) and b) of the four phenotypes in human esophageal cancer (h-ESO) and canine lymphoma (c-BCL) samples. Similarity matrix c) and d) calculated as the correlation between well-based feature vectors from all wells after unsupervised hierarchical clustering by phenotype. Note that the number of samples that fall into each phenotype is not the same for h-ESO and c-BCL.

Our interpretation of this improvement is that the red shift in the low frequency correlates with a decrease in average intracellular metabolic activity over the duration of the 10-hour assays, which in turn may be interpreted as an overall reduction in sample health. This is not surprising because the process of pinch biopsy, and division of the biopsy samples into small pieces, cause trauma of the sample. The red-shifted samples are likely samples whose overall health was already declining prior to drug application.

4. DISCUSSION

Biodynamic Imaging successfully demonstrates its ability to predict effective treatment for two distinct host and tumor types, and hints at possible existence of universal signatures that allow us to identify tumor phenotypes across different host species and tumor types. Both the predictive capability of BDI, and the universal signatures obtained from BDI, have important implications for general adoption of our technique in cancer therapy.

First, BDI demonstrates again that it is capable of identifying and predicting effective treatment for patient outcome under different chemotherapeutic treatments. Combined with the previous success BDI has seen with other tumor types, our findings suggest that BDI is not a niche technique only applicable to a narrow range of tumors, but rather a generally method that can be applied in a broad range of applications.

Second, previously, each host species and cancer type required enough replicate data to first construct a full drug-response library, before prediction of patient outcomes could be performed. This required significant time and resources and therefore posed a high barrier before competent predictions could be performed in clinical

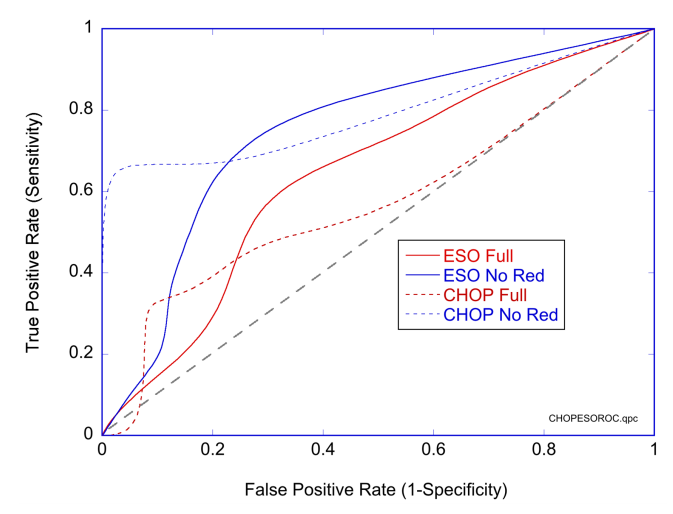


Figure 5. Human Esophageal (ESO) and Canine B-cell Lymphoma (CHOP) ROC curves when using all wells (Full) and when excluding redshifted wells (No Red) during double-hold-out cross-validation of patient predictions. Performance improves when the redshifted wells are removed: ESO: Full AUC = 0.64, No-Red AUC = 0.75; c-BCL: Full AUC = 0.57, No-Red AUC = 0.79.

settings. However, the existence of universal features or behaviors across multiple species and diseases provides an opportunity for transfer learning, eliminating the need for biodynamic imaging to be repeated exhaustively for each new disease indication, significantly reducing the upfront cost required to enable applications in clinical oncology.

ACKNOWLEDGMENTS

This work was supported by the National Science Foundation grant CBET-2200186.

REFERENCES

- [1] Yu, P., Peng, L., Mustata, M., Nolte, D. D., Turek, J., Melloch, M. R., Dunsby, C. W., Gu, Y., and French, P. M., "Imaging of tumor necroses using full-frame optical coherence imaging," in [Coherence Domain Optical Methods and Optical Coherence Tomography in Biomedicine VII], 4956, 34–41, SPIE (2003).
- [2] Yamaguchi, I., "Phase-shifting digital holography: Principles and applications," Digital holography and three-dimensional display: principles and applications, 145–171 (2006).
- [3] Cuche, E., Bevilacqua, F., and Depeursinge, C., "Digital holography for quantitative phase-contrast imaging," *Optics letters* **24**(5), 291–293 (1999).
- [4] Li, Z., Sun, H., Turek, J., Jalal, S., Childress, M., and Nolte, D. D., "Doppler fluctuation spectroscopy of intracellular dynamics in living tissue," *JOSA A* **36**(4), 665–677 (2019).
- [5] Choi, H., Li, Z., Sun, H., Merrill, D., Turek, J., Childress, M., and Nolte, D., "Biodynamic digital holography of chemoresistance in a pre-clinical trial of canine b-cell lymphoma," *Biomedical optics express* **9**(5), 2214–2228 (2018).
- [6] Li, Z., An, R., Swetzig, W. M., Kanis, M., Nwani, N., Turek, J., Matei, D., and Nolte, D., "Intracellular optical doppler phenotypes of chemosensitivity in human epithelial ovarian cancer," Scientific reports 10(1), 17354 (2020).
- [7] Laviana, A. A., Schiftan, E. G., Mashni, J. W., Large, M. C., Kaimakliotis, H. Z., Nolte, D. D., Turek, J. J., An, R., Morgan, T. A., and Chang, S. S., "Biodynamic prediction of neoadjuvant chemotherapy response: Results from a prospective multicenter study of predictive accuracy among muscle-invasive bladder cancer patients," in [Urologic Oncology: Seminars and Original Investigations], 41(6), 295–e9, Elsevier (2023).
- [8] Nolte, D. D., An, R., Turek, J., and Jeong, K., "Tissue dynamics spectroscopy for phenotypic profiling of drug effects in three-dimensional culture," *Biomedical optics express* **3**(11), 2825–2841 (2012).